LASER INTERFEROMETER GRAVITATIONAL WAVE OBSERVATORY
-LIGO-
CALIFORNIA INSTITUTE OF TECHNOLOGY
MASSACHUSETTS INSTITUTE OF TECHNOLOGY

Technical Note **LIGO-T040081- 01- R** 5/28/04

Lock Acquisition Scenario for the 40m Detuned RSE Prototype I. Central Part

S. Kawamura and O. Miyakawa

This is an internal working note
of the LIGO Project.

California Institute of Technology
LIGO Project – MS 51-33
Pasadena CA 91125
Phone (626) 395-2129
Fax (626) 304-9834
E-mail: info@ligo.caltech.edu

Massachusetts Institute of Technology
LIGO Project – MS 20B-145
Cambridge, MA 01239
Phone (617) 253-4824
Fax (617) 253-7014
E-mail: info@ligo.mit.edu

WWW: http://www.ligo.caltech.edu

File /home/blacke/documents/T9000xx.ps – printed November xx, 1999

ABSTRACT

The lock acquisition scenario for the 40m detuned resonant sideband extraction prototype is presented, with a focus on the central part of the interferometer.

1. Introduction

Lock acquisition of the 40m Detuned Resonant Sideband Extraction (DRSE) interferometer is one of the most important hurdles for us to clear to demonstrate the feasibility of this scheme for Advanced LIGO.

Several fixed-mass DRSE interferometers have been already successfully locked and operated[1,2,3,4,5]. A suspended-mass non-detuned RSE without a power recycling mirror[6], a suspended-mass DRSE without a power recycling mirror[7], the central part of a suspended-mass DRSE without a power recycling mirror[8], and a suspended-mass Detuned Dual Recycled (DDR) interferometer without arm cavities[9] also have been locked and operated. However, no suspended-mass full DRSE was yet tried. Difficulties in the lock acquisition of the suspended-mass full DRSE arise mainly in its larger number of degrees of freedom (DOF) to control compared with a power recycled Fabry-Perot Michelson interferometer, the larger velocity of the suspended masses compared with a fixed mass interferometer, and the anti-resonant status of the carrier inside the power recycling cavity by itself compared with a no-arm-cavity DDR. These complications make it impossible to simply apply the lock acquisition scheme used for the existing interferometers, including LIGO, GEO, TAMA, and the R&D prototypes described above, to the suspended-mass full DRSE.

Here we present a promising lock acquisition scenario for the 40m DRSE interferometer, especially for the central part of the interferometer. This method should be tried in the real system as soon as we obtain all the necessary hardware and software tools.

2. Brief review of the 40m DRSE interferometer

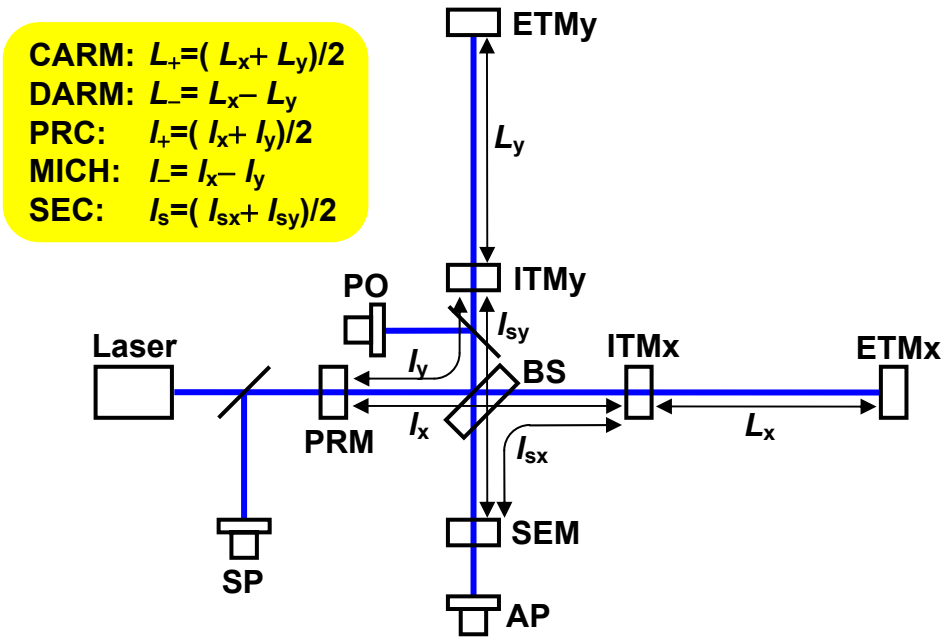

Fig. 1. Schematic diagram of the 40m DRSE interfeometer.

The 40m DRSE consists of two input test masses (ITMx and ITMy), two end test masses (ETMx and ETMy), a beam splitter (BS), a power recycling mirror (PRM), and a signal extraction mirror (SEM) illuminated by a laser beam as shown in エラー! 参照元が見つかりません。. It has five DOFs of length to control: L_+, L_-, l_+, l_-, and l_s as defined in Fig. 1. There are three optical ports, where we can obtain the length signals from: a symmetric port (SP), an asymmetric port (AP), and a pick-off port (PO). Note that the PO available at present is for the light coming from the BS to the ITMy. The light picked off at this port is slightly different from the light conventionally picked off, that is, the light coming from the BS to the PRM; the light picked off at the current PO is the combined light of the

light conventionally picked off, the light incident to the PRM from laser, and the light reflected by the SEM.

The laser light is phase-modulated at two different frequencies: f_1=33 MHz and f_2=166 MHz as shown in Fig. 2. This allows us to obtain length signals using a single demodulation (SDM: beats between carrier and f_1 or f_2) and a double demodulation (DDM: beats at $f_1 + f_2$ and $f_1 - f_2$, combined together). The Michelson macroscopic asymmetry is set in such a way that the $+f_2$ sideband incident to the BS is all reflected to the other BS port when the carrier incident to the BS is all reflected back to the same BS port. The macroscopic length of the power recycling cavity (PRC) is set in such a way that all the sidebands, both $\pm f_1$ and $\pm f_2$, are resonant when the carrier is anti-resonant in the PRC by itself (See the lower left figure of Fig. 2). Note that the carrier is, of course, resonant in the PRC cavity when the carrier is resonant in the arm cavities because of the phase flipping due to the arm cavities. The macroscopic length of the signal extraction cavity (SEC) is set in such a way that the $+f_2$ sideband is exactly anti-resonant when the carrier is appropriately detuned from resonance in the SEC (See the lower right figure of Fig. 2) Also note that the phase of the $+f_2$ sideband is advanced by $\pi/2$ when it is reflected from one BS port to the other BS port due to the macroscopic Michelson asymmetry, thus the round-trip phase advance due to this effect is π. These conditions make the $+f_2$ sideband resonant in the combined cavity consisting of the PRC and SEC. Note that the $-f_2$ sideband is not resonant in the combined cavity because of the detuning. On the other hand $\pm f_1$ sidebands are resonant only in the PRC and leak into the SEC only slightly. It is important to note that this scheme can be brought over to Advanced LIGO with minor modifications, f_1=9 MHz, f_2 = 180 MHz, to account for the longer PRC and SEC lengths at the sites.

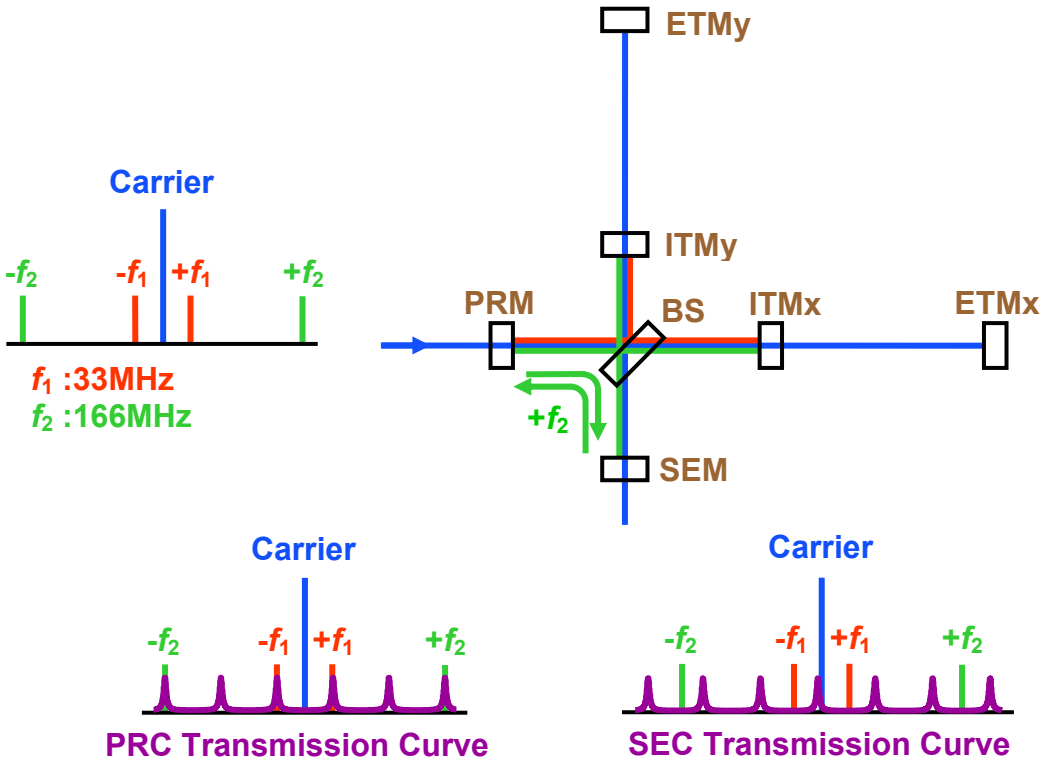

Fig. 2. Two phase modulations and macroscopic optical configuration.

3. Lock acquisition strategy

The lock acquisition strategy we take here is very simple: we lock one DOF at a time until we lock all the five DOFs. We lock the first DOF, and it should be robust even though the other four DOFs are free. Then we lock the second DOFs, and it should be robust even though the other three DOFs are free. We continue locking the remaining DOFs just one by one until all the DOFs are locked.
This approach is very different from the approach taken for the lock acquisition of the initial LIGO, where although each lock is not robust enough the next lock is accomplished with the aid of lock acquisition software quickly before the first lock is lost. We believe that the approach presented here is more suitable especially in the R&D phase. Only question is, then, whether or not such well-behaving signals can exist.

4. Overall lock acquisition scenario

In order to realize this strategy we first divide the lock acquisition procedure of the whole interferometer into the following two stages as shown in Fig. 3.

1. Lock the central part of the interferometer consisting of the ITMs, BS, PRM, and SEM using beats between f_1 and f_2
2. Lock the arm cavities consisting of the ITMs and ETMs using beats between carrier and f_1 or f_2

We believe that the lock of the central part of the interferometer is maintained when the arm cavities are locked. If the carrier were used to lock the central part, the polarity of the control signal would be flipped when the arm cavities are locked. Thus we should lose the lock of the central part. However, the amplitude and polarity of the signals for the central part obtained only from the sidebands do not depend on whether the arm cavities are locked or not, because the sidebands are not resonant in the arm cavities when the arm cavities are locked. Therefore the lock of the central part with this scheme cannot be lost when the arm cavities are locked.

We even believe and hope that the lock of the central part is robust even if the arm cavities are freely swinging. The worry is that occasional flashing of the sidebands in the arm cavities will vary the amplitude and possibly even the polarity of the signals obtained from the sidebands, which could potentially make the central part to fall out of lock. Nevertheless we think that the disturbances are probably too fast to cause loss of lock thanks to the high finesse of the arm cavities. We are also encouraged by the fact that TAMA300 demonstrated that the lock of the central part (a power recycled Michelson) with the signals obtained from the third harmonic demodulation (beats between the first-order sideband and the negative second-order sideband, and between the negative first-order sideband and the second-order sideband) was robust even when the arms cavities were freely swinging.

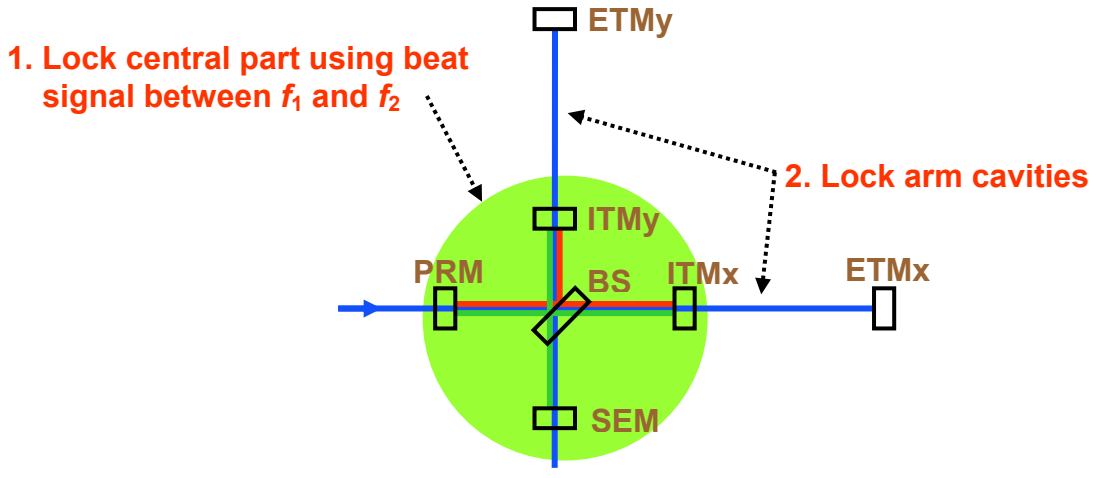

Fig. 3. Two stages of the lock acquisition.

5. Lock acquisition of central part

The lock of the central part can be attempted with the both arm cavities blocked using optical flags between the ITMs and ETMs. That way we can concentrate on the lock of the central part without any (if any) disturbances from the arm cavities. Once the central part is locked only with the sidebands we should unblock the arm cavities to see if the lock of the central part is maintained.

The lock of the central part can be acquired by the following steps:

(1) Lock l_- using a dither signal
(2) Lock l_+ using a DDM signal
(3) Lock l_s using a DDM signal
(4) Switch the l_- control signal from the dither signal to a DDM signal

The reason why the dither signal is introduced is because we found that no DDM signals are robust enough to maintain the lock of the first DOF while the other two DOFs are freely swinging. Even the best DDM signal (l_+) gives a sensible signal for only 80% of a possible pair of l_- and l_s (Fig. 4). The polarity of the signal will be flipped from time to time depending on l_- and l_s, which makes it impossible to maintain the lock with this signal.

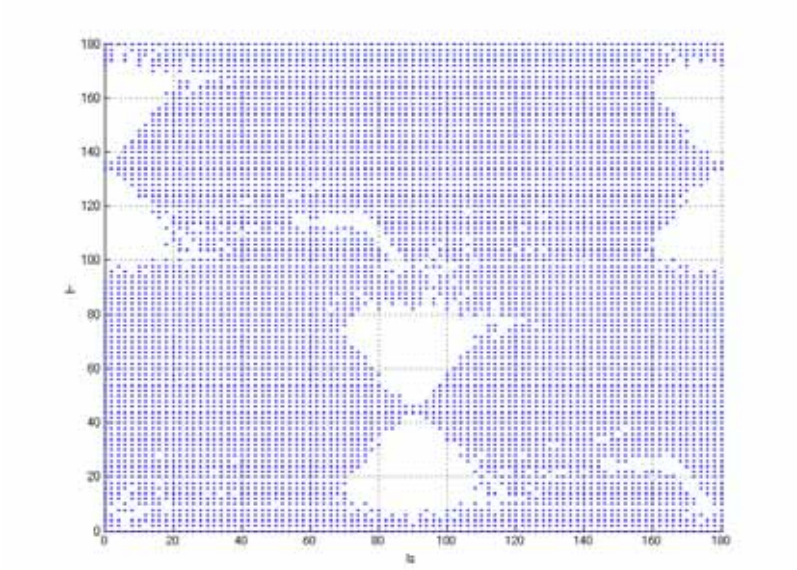

Fig. 4. Quality of the DDM signal l_+ depending on l_- and l_s. The dotted point represents a good signal, while space indicates that the signal is very poor. The horizontal axis is the phase of l_s, and the vertical axis is the phase of l_-, both in degrees. Initially, the interferometer is swinging freely through all values of these phases.

5-1. Lock l_- using a dither signal

The error signal to lock l_- is obtained by the dither method. To obtain a clean signal, we should turn off the RF modulations, which will be turned on later for the lock of l_+. We shake the two ITMs differentially at a few kHz. As shown in Fig. 5, we detect the light power at the PO and AP: V_{PO} and V_{AP}, and demodulate the signals with the dither frequency to obtain (V_{PO})' and (V_{AP})'. We calculate the following error signal in the front-end length sensing computer.

$$(V_{l-})' = \frac{(V_{AP})' V_{PO} - V_{AP}(V_{PO})'}{{V_{PO}}^2}$$

This signal is the derivative of the following signal with respect to l_-

$$V_{l-} = \frac{V_{AP}}{V_{PO}}$$

Note that all the signals, V_{PO}, V_{AP}, (V_{PO})', and (V_{AP})' are low-pass-filtered to remove the components at the dither frequency before doing the math. Incidentally if the light coming from the PRM to the BS were available to pick off ((a) in Fig. 5), $V_{AP}/V_{(a)}$ and its derivative with respect to l_- could be used instead. These signals are slightly better in quality than the existing signals. However, since these signals are not available in the current configuration of the 40m, we should stick to the existing pick-off port.

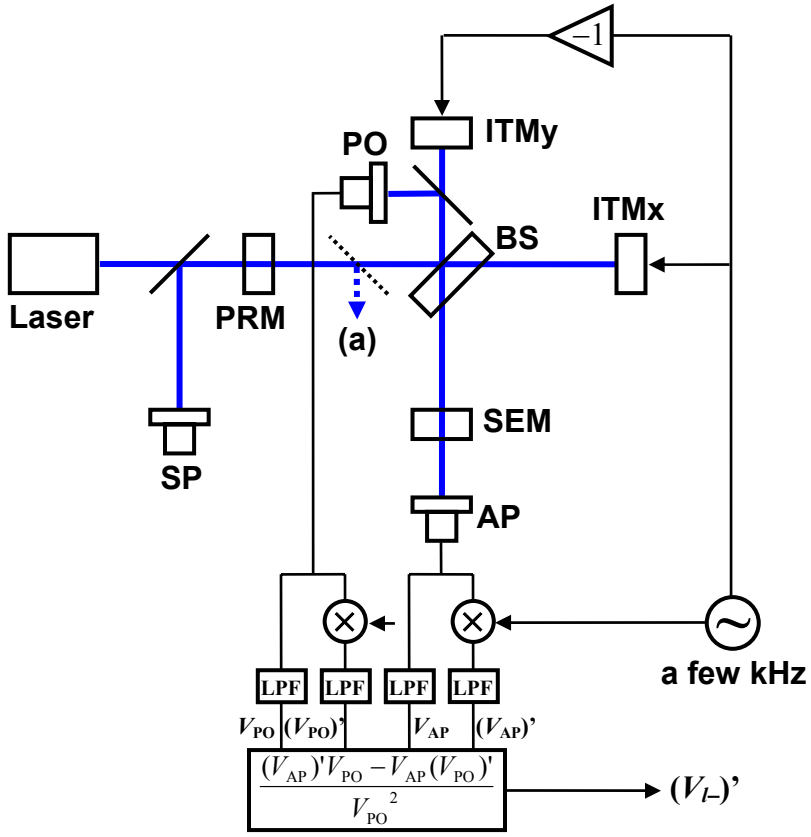

Fig. 5. l_- signal obtained by the dither method.

It was found by the FINESSE simulation that V_{l-} is equal to zero not depending on l_+ and l_s only if l_- is at the ideal microscopic position ($l_- = 0°$). This can be intuitively understood because the carrier incident to the BS is all reflected back to the same BS port (SP) when $l_- = 0°$; thus $V_{AP} = 0$. It was also found that l_-–dependence of V_{l-} does not depend on l_+ at all but only depends on l_s (Fig. 6). Note that V_{l-} has a very large value at a certain value for l_- depending on l_s (Fig. 7). We will explain later that this is probably not a problem.

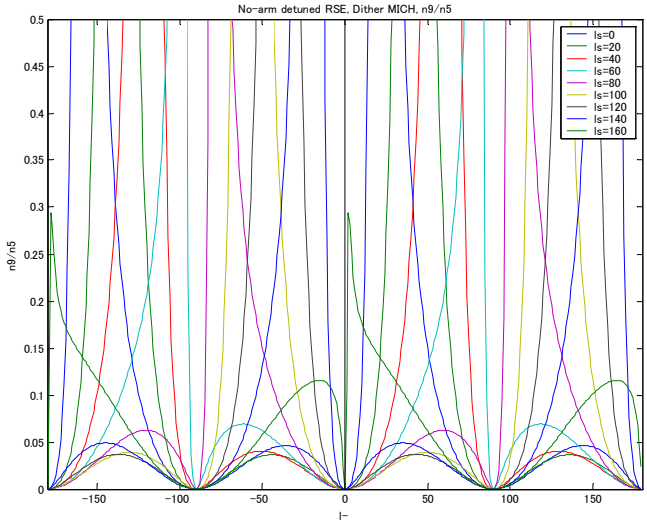

Fig. 6. Dependence of the V_{l-} signal on l_- with various values of l_s. The horizontal axis is the phase of l_- in degrees (-180° < l_- < +180°), and the vertical axis is V_{l-} in arbitrary unit (0 < V_{l-} < +0.5). The phase of l_s for each curve is 0°, 20°, 40°, 60°, 80°, 100°, 120°, 140°, 160°, respectively. The curves do not depend on l_+ at all.

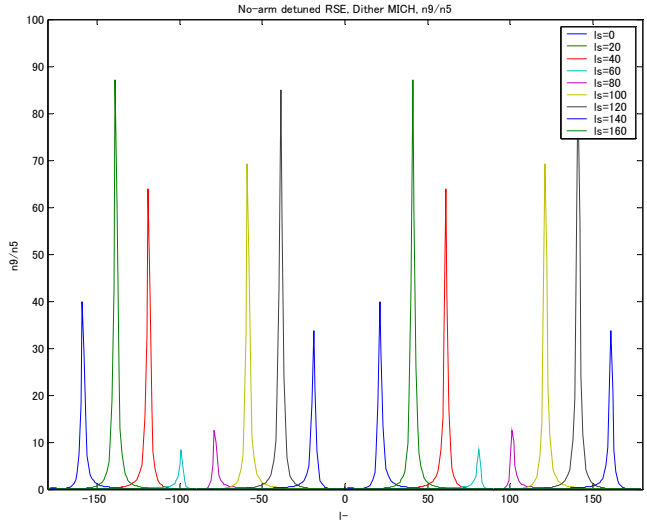

Fig. 7. Dependence of the V_{l-} signal on l_- with various values of l_s. The horizontal axis is the phase of l_- in degrees (-180° < l_- < +180°), and the vertical axis is V_{l-} in arbitrary unit (0 < V_{l-} < +100). The phase of l_s for each curve is 0°, 20°, 40°, 60°, 80°, 100°, 120°, 140°, 160°, respectively. The curves do not depend on l_+ at all.

Since V_{l-} has a minimum value at $l_- = 0°$, the derivative of V_{l-} with respect to l_- should give a good linear signal around $l_- = 0°$. This signal, $(V_{l-})'$, also does not depend on l_+ at all but only depends on l_s. The outstanding advantage of this signal is that its slope around $l_- = 0°$ is of the same polarity for any l_s as shown in Fig. 8 and Fig. 9. Note that the $(V_{l-})'$ signal also crosses zero with a slope of the same polarity at $l_- = \pm 90°$, which is not a desirable locking point. This point also gives the dark-fringe-at-AP condition. However, the carrier is opposite in phase compared with that for the ideal point ($l_- = 0°$), the status of the carrier in the PRC+SEC combined cavity at $l_- = \pm 90°$ is always opposite to that for the ideal point. Therefore with a chance of 50%, we could lock to the undesirable point. Also note that this signal has a huge error signal around a certain value of l_- depending on l_s (Fig. 10), which corresponds to the huge peaks in Fig. 7. Fortunately, however, the slope of this signal is opposite to the slope of the desirable error signal. Thus it can never be locked to those points with a proper polarity of the servo system, although we should probably limit the signal range to remove the disturbances of those undesirable error signals.

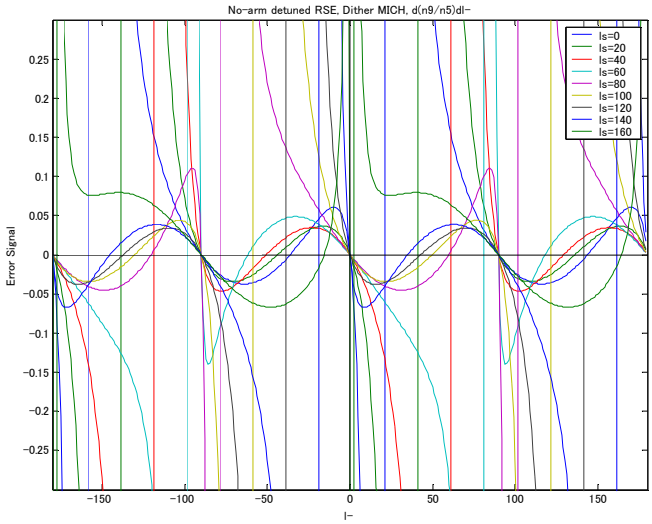

Fig. 8. Dependence of the $(V_{l-})'$ signal on l_- with various values of l_s. The horizontal axis is the phase of l_- in degrees ($-180° < l_- < +180°$), and the vertical axis is $(V_{l-})'$ in arbitrary unit ($-0.3 < (V_{l-})' < +0.3$). The phase of l_s for each curve is 0°, 20°, 40°, 60°, 80°, 100°, 120°, 140°, 160°, respectively. The curves do not depend on l_+ at all.

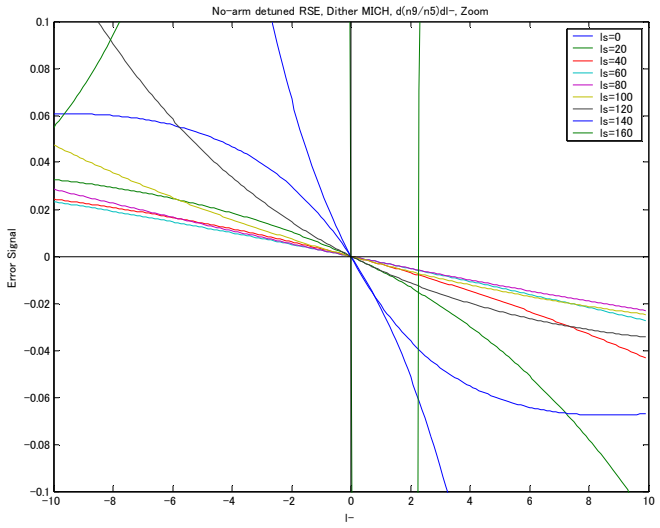

Fig. 9. Dependence of the (V_{l-})' signal on l_- with various values of l_s. The horizontal axis is the phase of l_- in degrees (-10° < l_- < +10°), and the vertical axis is (V_{l-})' in arbitrary unit (-0.1 < (V_{l-})' < +0.1). The phase of l_s for each curve is 0°, 20°, 40°, 60°, 80°, 100°, 120°, 140°, 160°, respectively. The curves do not depend on l_+ at all.

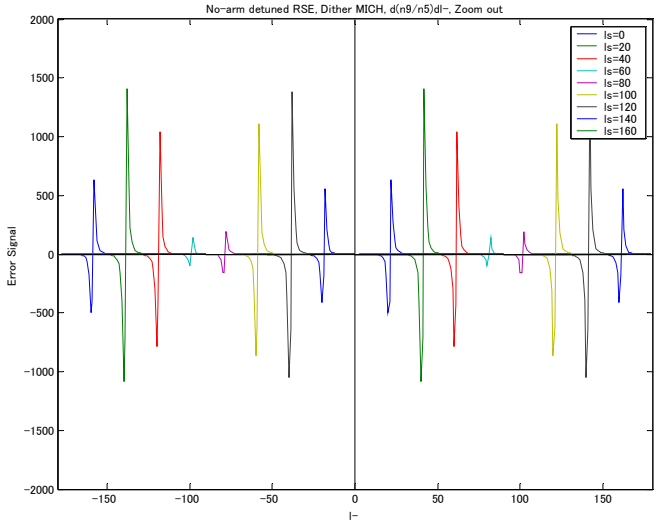

Fig. 10. Dependence of the (V_{l-})' signal on l_- with various values of l_s. The horizontal axis is the phase of l_- in degrees (-180° < l_- < +180°), and the vertical axis is (V_{l-})' in arbitrary unit (-2000 < (V_{l-})' < +2000). The phase of l_s for each curve is 0°, 20°, 40°, 60°, 80°, 100°, 120°, 140°, 160°, respectively. The curves do not depend on l_+ at all.

Although the slope of the (V_{l-})'signal has the same polarity for any l_s, the slope of the error signal varies significantly depending on l_s as shown in Fig. 11. The servo system for the l_- lock should be designed in such a way that the system is as stable as possible with this varying control loop gain. Nevertheless the system would probably experience an oscillation for l_s that gives too high gain. We still hope that the oscillation could happen in such a short period that it cannot cause unlocking of the system. If the oscillation causes unlocking, we could implement a limiter that could prevent a large oscillation.

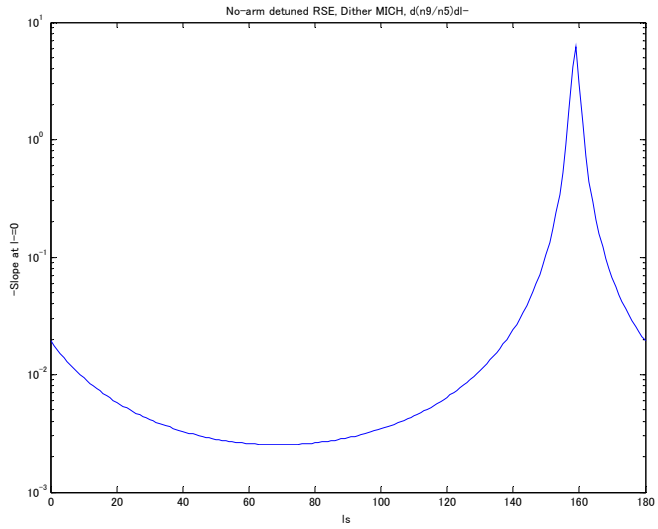

Fig. 11. Dependence of the slope of the (V_{l-})' signal at $l_- = 0°$ on ls. The horizontal axis is the phase of l_s in degrees ($0° < l_s < +180°$), and the vertical axis is the slope of (V_{l-})' at $l_- = 0°$ in logarithmic arbitrary unit ($10^{-3} < (V_{l-})' < 10^{1}$).

Another concern of the (V_{l-})' signal is that the signal quality is degraded by the existence of the RF modulations. Fig. 12 and Fig. 13 show the dependence of the (V_{l-})' signal on l_- with the RF modulations of m=0.01 and m=0.03, respectively. It can be seen that the demodulation disturbs both the slope and zero-crossing of l_-. It seems that the disturbances are not so crucial with a modulation depth of 0.01, but significantly worse with a modulation depth of 0.03. After l_- is locked we should gradually increase the modulation depth to see how much modulation depth we could have without kicking the system out of lock and to see if that modulation depth is large enough to obtain sensible signals for the next steps.

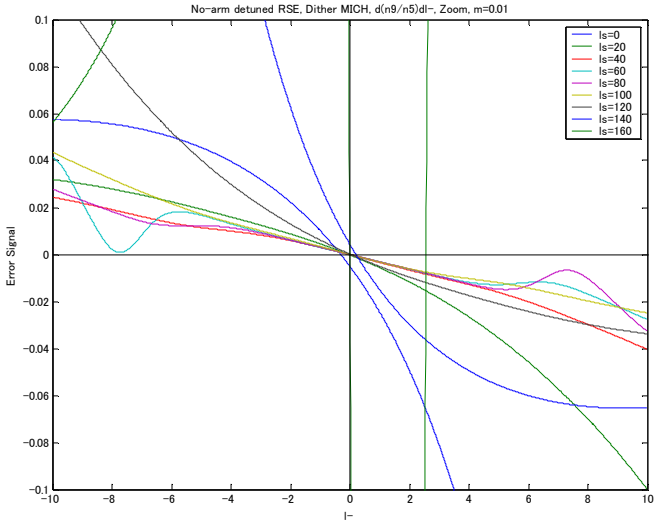

Fig. 12. Dependence of the (V_{l-})' signal on l_- with the existence of the RF modulations (m=0.01) with various values of l_s. The horizontal axis is the phase of l_- in degrees (-10° < l_- < +10°), and the vertical axis is (V_{l-})' in arbitrary unit (-0.1 < (V_{l-})' < +0.1). The phase of l_s for each curve is 0°, 20°, 40°, 60°, 80°, 100°, 120°, 140°, 160°, respectively. The curves do not depend on l_+ at all.

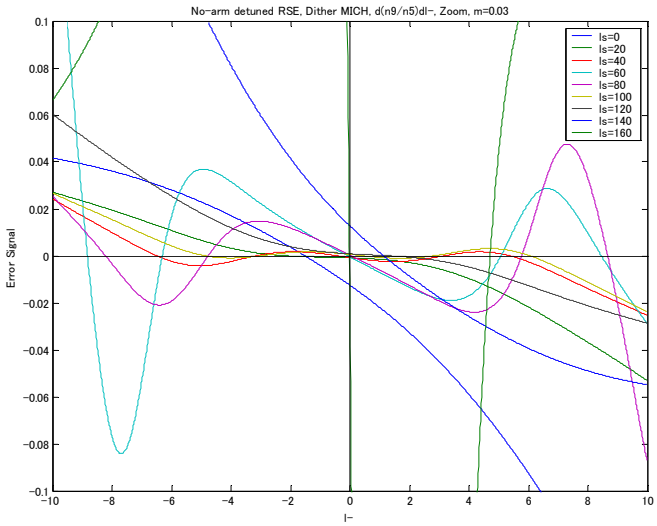

Fig. 13. Dependence of the (V_{l-})' signal on l_- with the existence of the RF modulations (m=0.03) with various values of l_s. The horizontal axis is the phase of l_- in degrees (-10° < l_- < +10°), and the vertical axis is (V_{l-})' in arbitrary unit (-0.1 < (V_{l-})' < +0.1). The phase of l_s for each curve is 0°, 20°, 40°, 60°, 80°, 100°, 120°, 140°, 160°, respectively. The curves do not depend on l_+ at all.

5-2. Lock l_+ using a DDM

From now on we assume that l_- is always locked to the ideal point ($l_- = 0°$). As the second step the error signal to lock l_+ is obtained by the DDM at SP. For the final operation, the DDM phases should be chosen to minimize the offset at $l_+ = 0°$ (when $l_s = 0°$) and to maximize the derivative of the DDM signal with respect to l_+ at $l_+ = 0°$ (when $l_s = 0°$)[10]. This is not the case, however, for the lock acquisition of l_+. The DDM error signal for l_+ with the DDM phases optimized for no offset and maximum l_+ does not cross zero for some l_s as shown in Fig. 14. This is obviously not good; the lock of l_+ cannot be maintained when l_s is freely swinging.

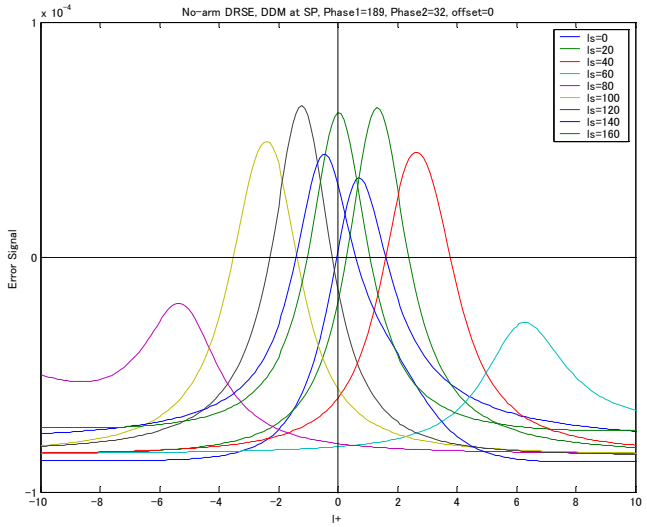

Fig. 14. Dependence of the DDM signal at SP on l_+ with various values of l_s. The DDM phases are chosen to minimize the offset at $l_+ = 0°$ (when $l_s = 0°$) and to maximize the derivative of the DDM signal with respect to l_+ at $l_+ = 0°$ (when $l_s = 0°$). The horizontal axis is the phase of l_+ in degrees ($-10° < l_+ < +10°$), and the vertical axis is the DDM signal in arbitrary unit. The phase of l_s for each curve is 0°, 20°, 40°, 60°, 80°, 100°, 120°, 140°, 160°, respectively. l_- is assumed to be locked to the ideal point ($l_- = 0°$).

Fortunately, however, we found that the DDM error signal for l_+ behaves well when the DDM phases are optimized to minimize the average offset instead of the offset at $l_+ = 0°$ (when $l_s = 0°$) and to maximize the derivative of the DDM signal with respect to l_+ at $l_+ = 0°$ (when $l_s = 0°$) as shown in Fig. 15. Note that the zero-crossing for l_+ depends on l_s. It means that the lock point of l_+ changes in accordance with l_s. This is fine because what we should do is to constrain a DOF, which does not have to be exactly equal to l_+. It also can be seen that the lock point of l_+ exactly follows the displacement of l_s. The reason is the following. This error signal is given by the condition that $+f_2$ sideband is resonant in the PRC+SEC combined cavity. When the l_- is locked to the ideal point, the carrier incident to the BS is all reflected back to the PRM, whereas the $+f_2$ sideband is all sent to the SEM. The $+f_2$ sideband is then reflected by the SEM, and sent to the PRM this time. Therefore the combined cavity for the $+f_2$ sideband practically becomes a simple cavity consisting of the PRM and SEM. Thus the PRM should exactly follow the motion of the SEM in order to keep the resonance condition of $+f_2$.

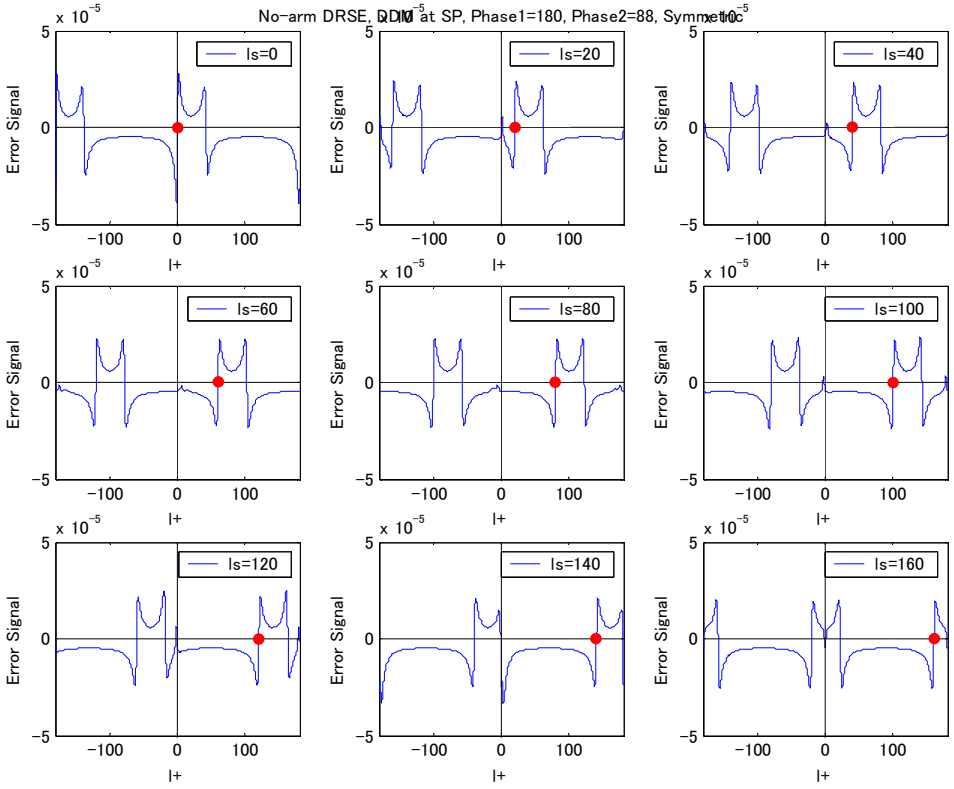

Fig. 15. Dependence of the DDM signal at SP on l_+ with various values of l_s. The DDM phases are chosen to minimize the average offset instead of the offset at $l_+ = 0°$ (when $l_s = 0°$) and to maximize the derivative of the DDM signal with respect to l_+ at $l_+ = 0°$ (when $l_s = 0°$). The horizontal axis is the phase of l_+ in degrees ($-180° < l_+ < +180°$), and the vertical axis is the DDM signal in arbitrary unit. The phase of l_s for each figure is 0°, 20°, 40°, 60°, 80°, 100°, 120°, 140°, 160°, respectively. l_- is assumed to be locked to the ideal point ($l_- = 0°$).

5-3. Lock l_s using the DDM

Now we assume that l_- is always locked to the ideal point ($l_- = 0°$) and l_+ is following the motion of l_s. As the third step the error signal to lock l_s is obtained by the DDM at PO. Here the DDM phases are chosen to minimize the offset at $l_s = 0°$ (when $l_+ = 0°$) and to maximize the derivative of the DDM signal with respect to l_s at $l_s = 0°$ (when $l_+ = 0°$). The obtained error signal is reasonable as shown in Fig. 16. Note that to produce the plot in this figure at each value of l_s the same value is assumed for l_+.

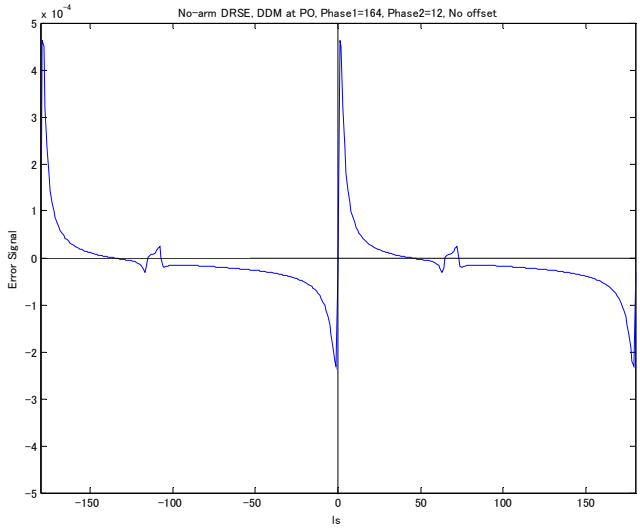

Fig. 16. Dependence of the DDM signal at PO on l_s. The DDM phases are chosen to minimize the offset at $l_s = 0°$ (when $l_+ = 0°$) and to maximize the derivative of the DDM signal with respect to l_s at $l_s = 0°$ (when $l_+ = 0°$). The horizontal axis is the phase of l_s in degrees ($-180° < l_s < +180°$), and the vertical axis is the DDM signal in arbitrary unit. l_- is assumed to be locked to the ideal point ($l_- = 0°$), and l_+ is assumed to follow l_s.

5-4. Switch the l_- control signal from the dither signal to the DDM signal

Now that all the three DOFs are locked, we can switch the l_- control signal from the dither signal to the DDM signal at AP. The DDM phases are chosen to minimize the offset at $l_- = 0°$ (when $l_+ = 0°$ and $l_s = 0°$) and to maximize the derivative of the DDM signal with respect to l_- at $l_- = 0°$ (when $l_+ = 0°$ and $l_s = 0°$). The obtained error signal is shown in Fig. 17. The smooth transfer of the control signal can be done using the conventional technique: superimpose the DDM signal to the dither signal, and then remove the dither signal.

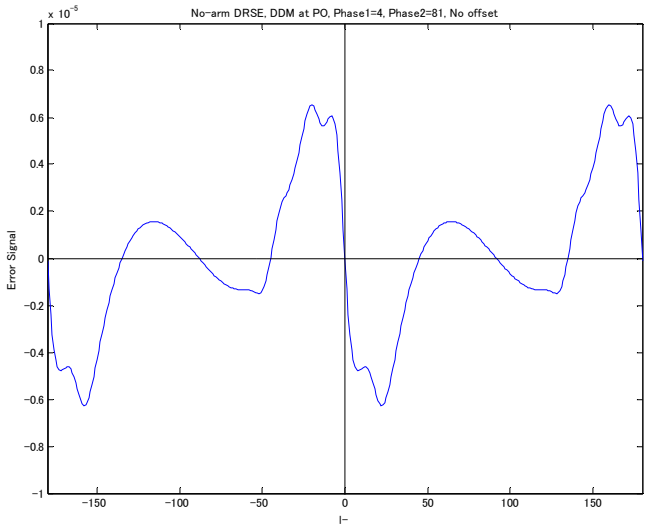

Fig. 17. Dependence of the DDM signal at AP on l_-. The DDM phases are chosen to minimize the offset at $l_- = 0°$ (when $l_+ = 0°$ and $l_s = 0°$) and to maximize the derivative of the DDM signal with respect to l_- at $l_- = 0°$ (when $l_+ = 0°$ and $l_s = 0°$). The horizontal axis is the phase of l_- in degrees ($-180° < l_- < +180°$), and the vertical axis is the DDM signal in arbitrary unit. l_+ and l_s are assumed to be locked to the ideal point ($l_+ = 0°$, $l_s = 0°$).

6. Lock acquisition of arm cavities

The lock acquisition of the arm cavities will be presented in a separate report.

References

[1] K. Strain, G. M¨uller, T. Delker, D. Reitze, D. Tanner, J. Mason, P. Willems, D. Shaddock, M. Gray, C. Mow-Lowry, and D. McClelland, Appl. Opt. **42** (2003) p.1244

[2] G. M¨uller, T. Delker, D. Tanner, and D. Reitze, Appl. Opt. **42**, (2003) p.1257

[3] J. Mason and P. Willems, Appl. Opt. **42**, (2003) p.1269

[4] D. Shaddock, M. Gray, C. Mow-Lowry, and D. McClelland, Appl. Opt. **42**, (2003) p.1283

[5] P. Beyersdorf, S. Kawamura, K. Somiya, F. Kawazoe, M. Agueros, "A prototype power-recycled RSE interferometer using polarization detection", submitted to Appl. Opt.

[6] O. Miyakawa, K. Somiya, G. Heinzel, and S. Kawamura, "Development of a Suspended-mass RSE interferometer Using Third Harmonic Demodulation", Class. and Quantum Gravity, **19** (2002) p.1555-1560

[7] K. Somiya, "Investigation of radiation pressure effect in a frequency-detuned interferometer and development of the readout scheme for a gravitational-wave detector", Doctor Thesis, 2004

[8] B. Barr, "Experimental Investigations into Advanced Configurations and Optical Techniques for Laser Interferometric Gravitational Wave Detectors", Doctor Thesis, 2003

[9] H. Grote, "Making it Work: Second Generation Interferometry in GEO600!", Doctor Thesis, 2003

[10] S. Kawamura "Signal Extraction Matrix of the 40m Detuned RSE Prototype", LIGO Internal Working Note, LIGO-T040010-00-R (2004)